Water Research 95 (2016) 310–318

Contents lists available at ScienceDirect

Water Research

journal homepage: www.elsevier.com/locate/watres

Effects of calcium and ferric ions on struvite precipitation: A new assessment based on quantitative X-ray diffraction analysis

Hanlu Yan, Kaimin Shih*

Department of Civil Engineering, The University of Hong Kong, Pokfulam Road, Hong Kong

ARTICLE INFO

Article history:
Received 14 September 2015
Received in revised form
6 March 2016
Accepted 13 March 2016
Available online 18 March 2016

Keywords:
Struvite
Crystallization
Quantitative XRD
Amorphous content

ABSTRACT

The precipitation of struvite ($MgNH_4PO_4 \cdot 6H_2O$) from waste streams has attracted considerable attention due to its potential for recovering phosphorus for fertilization. As struvite is primarily acquired by means of precipitation and crystallization from aqueous solutions, it is important to evaluate the roles of common metal ions, particularly those that are commonly found in wastewater, in the struvite crystallization process. This study was performed to quantitatively evaluate the effects of calcium and ferric ions on struvite crystallization using the Rietveld refinement method, which is based on the analysis of X-ray diffraction data. The results indicate that both calcium and ferric ions significantly inhibit the formation of struvite crystals, and the effects vary under different pH conditions. There was a negative linear correlation between the struvite weight content in the precipitates and the Ca/Mg molar ratio in the initial solution. However, ferric ions were confirmed to be a more efficient inhibitor of struvite crystallization. Ca^{2+} and Fe^{3+} further modified the needle-like struvite into irregular shapes. An unambiguous and quantitative understanding of the effects of foreign ions on struvite crystallization will help to reliably improve the quality of struvite products recovered from wastewater and the control of struvite deposits in water and sludge piping systems.

1. Introduction

Struvite (MAP, $MgNH_4PO_4 \cdot 6H_2O$) crystallization is one of the main mechanisms that can lead to severe clogging problems in the sludge piping systems of many wastewater treatment plants (WWTPs). Struvite was first identified as a crystalline material by Rawn in a study of municipal wastewater digestion problems (Rawn et al., 1939). Since then, pipe blockages due to struvite deposition in wastewater treatment plants have been commonly reported (Pitman et al., 1991; Williams, 1999; Borgerding, 1972), resulting in the need to replace pipework (Ohlinger et al., 1998). However, the formation of struvite is also considered to be a highly promising strategy for recovering phosphorus (P) as a potential slow-release fertilizer. These high-quality struvite materials have been widely tested for their nutrient leaching properties and are considered to be suitable for fertilizer application, particularly in moderately alkaline and acidic soils (Massey et al., 2007). Struvite is a convenient source of nitrogen (N) and P from wastewater, and with the rapid depletion of phosphate rock resources, it could be applied as an ecofertilizer to compete against traditional fertilizers if its crystallization process could be well controlled (Rahman et al., 2014).

The struvite crystallization process includes nucleation and crystal growth processes that are affected by physicochemical factors such as the pH, supersaturation ratio, temperature, and mixing, and by the existence of foreign ions. Among these factors, few studies have focused on the influences of foreign ions on struvite crystallization (Le Corre et al., 2009). Kabdaszli et al. (2006) evaluated the effects of Na^+, SO_4^{2-}, CO_3^{2-}, and Ca^{2+} on the induction time of struvite precipitation. All of the tested ions clearly retarded the struvite crystallization, except for a very minor effect observed for the carbonate ions. Le Corre et al. (2005) undertook a series of struvite precipitation experiments to assess the effect of calcium ions on the struvite shape, crystal size, and purity. The pH was measured during the entire process and was used as an indicator of the struvite formation rate. The purity of struvite was analyzed by energy dispersive X-ray spectroscopy (EDS) to provide a comparison of the elemental distribution. Muryanto and Bayuseno (2014) investigated the struvite crystallization kinetics with interference from Zn^{2+} and Cu^{2+} and found that both ions at ppm levels can

* Corresponding author.
E-mail address: kshih@hku.hk (K. Shih).

http://dx.doi.org/10.1016/j.watres.2016.03.032
0043-1354/

inhibit the struvite crystallization rate and that Zn^{2+} was a more effective antiscalant for struvite control. In our study, calcium ion was selected to observe its influence on struvite crystallization because calcium is often observed in the wastewater treatment process, particularly in settled sludge liquors (Ca/Mg molar ratio ranging from 1.4 to 3.7) (Parsons et al., 2001). Moerman et al. (2009) reported intensive interference from calcium in the formation of struvite and the phosphorus removal efficiency from pilot- and full-scale agro-industry wastewater. Calcium phosphate precipitation is regarded as another essential route of phosphorus removal and recovery. It is thus crucial to accurately report the composition of products achieved from solutions that contain Ca^{2+} and Mg^{2+}. Iron (Fe) chemicals are commonly used in wastewater treatment for coagulation, flocculation, and removal of phosphorus. In particular, ferric salts have been dosed into sludge anaerobic digestion systems to control the emission of hydrogen sulfide (H_2S) into biogas (Charles et al., 2006; Ge et al., 2012; Gutierrez et al., 2010). Ferric ions are widely known for their effects on crystal growth, such as the alteration of needle-shaped $NH_4H_2PO_4$ crystals into tapered prisms (Mullin, 1972). This method has been used to control struvite scale formation in anaerobic sludge digesters (Mamais et al., 1994). Therefore, this work focuses on calcium and ferric ions as they have a high potential to co-exist in struvite precipitation, which normally involves a combination of enhanced biological phosphorus removal (EBPR) and sludge digestion techniques (Battistoni et al., 2002; Cusick et al., 2014; Musvoto et al., 2000).

Although previous studies have identified various characteristics of struvite products derived from a wide variety of solution compositions, much less work has been done to provide information on the phase composition of struvite-containing precipitates. In this study, the phase compositions of products obtained from P-enriched solutions were directly analyzed by quantitative X-ray diffraction (QXRD) to quantify the effects of calcium and ferric ions on struvite crystallization. Together with scanning electron microscope (SEM) and Raman testing, a scientific understanding of the struvite crystallization mechanism and crystal growth behavior will provide a promising avenue for the effective recovery of quality struvite products from waste streams as a renewable nutrient resource.

2. Materials and methods

2.1. Batch experiments

Analytical grade magnesium chloride hexahydrate ($MgCl_2 \cdot 6H_2O$), ammonium chloride (NH_4Cl), and potassium dihydrogen phosphate (KH_2PO_4) were selected to produce struvite precipitation. The chemicals were dissolved in distilled water to prepare stock solutions at a concentration of 0.1 M. $CaCl_2$ and $FeCl_3$ were used to investigate the influences of calcium and ferric ions on struvite crystallization. In each experiment, 100 mL stock solutions of $MgCl_2$, NH_4Cl, and KH_2PO_4 were agitated in a 600 mL beaker at a fixed rotation speed, with the molar ratio of Mg, N, and P fixed at 1:1:1. For the calcium ion influence experiments, the molar ratios of Ca to Mg were designated as 1:5, 1:3, 1:2, 1:1, 1.25:1, and 2:1, and the experiments were performed under a wide pH range (7.5, 8.0, 9.0, 10.0, and 11.0), which has been suggested as the possible condition for struvite precipitation based on a variety of wastewater-derived sources (Wang et al., 2005). For the ferric ion influence experiments, the Fe^{3+} dosages were designated as 1 ppm, 5 ppm, 100 ppm, 200 ppm, and 372 ppm, with an Fe/Mg molar ratio of 1:5, at two pH values (7.5 and 9.0) due to the limited solubility of ferric compounds in alkaline conditions and strong flocculation properties. The initial pH of the mixture solution was acidic (pH 4.2 ± 0.1), so 1 M NaOH solution was added to adjust the system pH to the designated values. The solutions were agitated for 30 min and allowed to settle for 12 h, followed by filtration of the precipitates through 0.45 μm filters. The precipitates were dried at room temperature for 2 days before the subsequent characterizations. The liquor samples were also collected for the elemental analysis.

2.2. Analytical methods

The precipitates derived from the processes mentioned above were ground into powder and examined by XRD to determine their phase compositions. A Bruker D8 diffractometer (Bruker Co. Ltd.) equipped with a Cu X-ray tube was used to collect the diffraction patterns in step sizes of 0.02°, ranging from 10° to 110° at a 2θ angle. XRD analysis was also used to quantify the phase compositions of the samples using the Rietveld refinement method by fitting the full-profile experimental XRD data with a calculated diffraction pattern (Wiles and Young, 1981; Young, 1993). More specifically, by adding internal standards in known proportions, the absolute abundance of crystalline phases and amorphous phase(s) in a mixed sample can be calculated through intensity fitting of the respective peaks (Guirado et al., 2000). Calcium fluoride (CaF_2) has no overlapping peaks with the studied phases and was chosen as the internal standard due to its high crystallinity. Topas 4-2 software (Bruker, Mannheim, Germany), which is based on the Rietveld refinement method, was used in this work to conduct the phase quantification task. Four reliability index parameters, i.e., the pattern factor (Rp), the weighted pattern factor (Rwp), the expected error (Rexp), and the goodness of fit (GOF), are commonly utilized to evaluate the quality of refinement work. They are defined by the following equations:

$$R_p = \frac{\sum |Y_i(obs) - Y_i(calc)|}{\sum Y_i(obs)} \quad (1)$$

$$R_{wp} = \left\{ \frac{\sum \omega_i [Y_i(obs) - Y_i(calc)]^2}{\sum \omega_i [Y_i(obs)]^2} \right\}^{\frac{1}{2}} \quad (2)$$

$$R_{exp} = \left\{ \frac{\sum N_d - N_p}{\sum \omega_i [Y_i(obs)]^2} \right\}^{\frac{1}{2}} \quad (3)$$

$$GOF = \frac{R_{wp}}{R_{exp}} \quad (4)$$

where Y_i(obs) and Y_i(calc) are the observed and calculated data at data point i, respectively; ω_i is the weighting given to data point i; N_d is the number of data points, and N_p is the number of parameters.

The linear regression analysis of the quantitative data was conducted using ORIGIN software (version 9.0). The morphology of the samples was observed with an SEM (Hitachi S-4800 FEG and LEO 1530 FEG SEM) combined with elemental mapping with an EDS system. The highly amorphous precipitates were also examined by Raman spectroscopy. The Raman spectra were measured on a Renishaw inVia Raman microscope (Renishaw, UK) using a He–Ne laser (633 nm, 17 mW). Phosphorus concentrations in the liquid samples were measured by UV spectrophotometry at 700 nm based on the molybdenum-blue ascorbic acid method. The concentrations of magnesium and calcium ions were determined by inductively coupled plasma–optical emission spectrometry (ICP-OES, Perkin Elmer Optima 8000).

3. Results and discussion

3.1. Influence of calcium ions on struvite crystallization

3.1.1. Quantitative analysis of calcium-affected precipitates by the Rietveld method

The dry precipitates obtained from the calcium influence experiments were first analyzed using XRD for phase identification. The obtained powder XRD patterns were compared to the data from the standard powder diffraction database of the International Centre for Diffraction Data (PDF-2, Release 2008). Struvite (PDF#71-2089) and hydroxyapatite (PDF#09-0432) were identified as the two phosphorus crystalline phases, and hydroxyapatite was only present in the highly amorphous samples precipitated at a Ca/Mg molar ratio of 2:1. As shown in Fig. 1 (patterns of samples obtained from the solution at pH 10.0), struvite was the only detectable phase in the precipitates and its intensity decreased as the initial Ca/Mg molar ratio increased. When the concentration of calcium was double that of magnesium, the struvite peaks disappeared, indicating that struvite crystallization was completely inhibited by calcium. Compared to the struvite standard pattern, the samples in this study were observed to have preferred orientations along the (002), (012), and (004) planes, even though all of the samples were thoroughly ground. The oriented growth of struvite crystals has been widely reported in previous studies, especially in studies of urinary calculi (Rouff, 2013; Wang et al., 2006; Sutor and Wooley, 1972). Therefore, all of the sample diffraction data were refined with the preferred orientation parameter. According to the comparison shown in Fig. 1, the preferred orientation of struvite was also inhibited by an increase in calcium interference.

On the basis of the phase identification outcome, the struvite samples precipitated from the calcium-containing solution provided a further opportunity to use the Rietveld method to quantify the phase abundances in the products. Fig. 2 presents an example of an XRD pattern (of a sample precipitated at pH 10.0 with a Ca/Mg mole ratio of 1:5) analyzed by Rietveld refinement and shows the agreements and differences between the observed and calculated diffraction patterns. The four reliability index parameters - Rp, Rwp, Rexp and GOF - which indicate the quality of refinement work in this study, are presented in Tables S1 and S2 in the supporting information. The ideal value for a GOF is 1.0, and all of the refinement work was observed to be of acceptable quality.

Based on the quantification results, we plotted the struvite contents in the precipitates versus the Ca/Mg molar ratios in the initial solution in Fig. 3. The results revealed that struvite crystallization was significantly inhibited by calcium ions, particularly at high pH values (pH ≥ 10). The struvite contents in the precipitates were generally below 50 wt% when the Ca:Mg molar ratio was 1:1 or higher. Moreover, a good linear correlation was found between the struvite weight contents (y, %) and the Ca/Mg molar ratios (x),

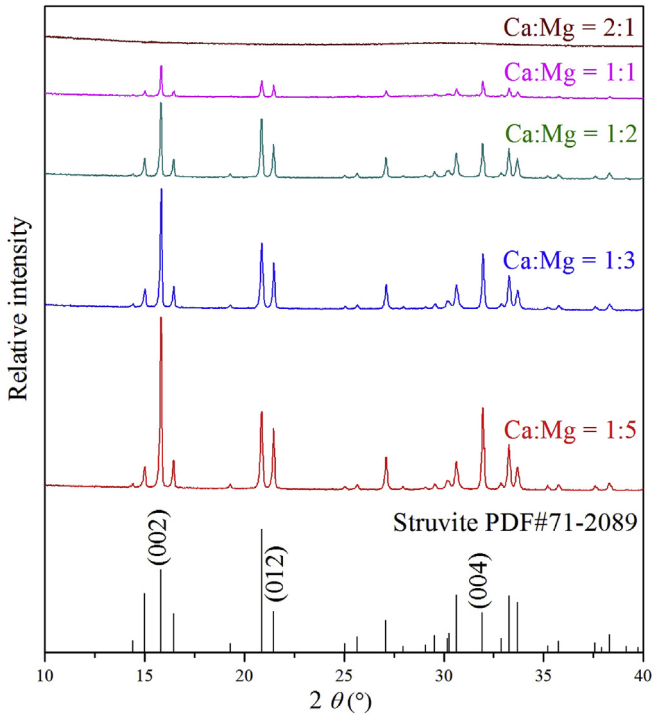

Fig. 1. XRD patterns of samples precipitated at pH 10.0 with different Ca/Mg molar ratios. The struvite standard pattern is also provided according to PDF #71-2089.

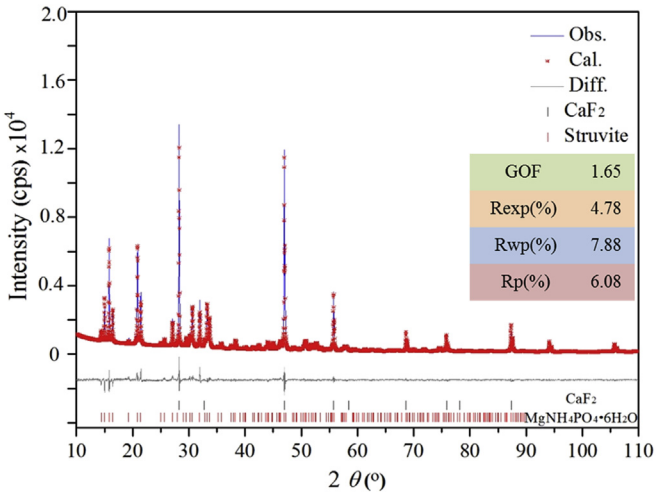

Fig. 2. Observed (blue line), calculated (red cross), and difference (grey line) curves of the refined pattern (sample precipitated at pH 10.0 with a Ca/Mg ratio of 1:5) with 25 wt% CaF_2 added as the internal standard. Vertical bars represent the Bragg positions of the calculated reflections for CaF_2 and struvite. Four commonly used reliability index parameters are also shown in the right side. (For interpretation of the references to colour in this figure legend, the reader is referred to the web version of this article.)

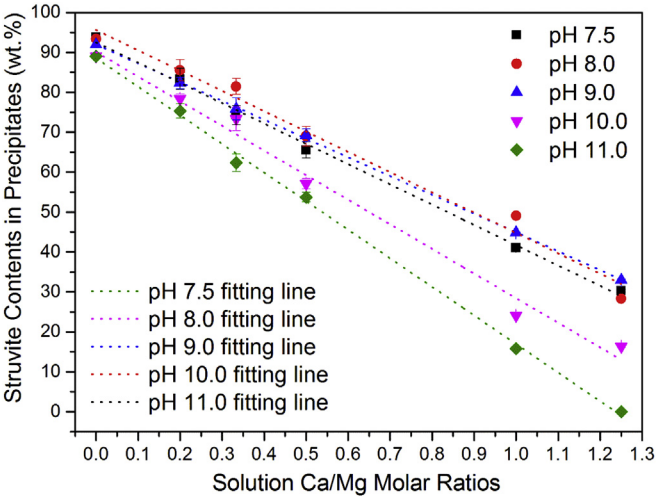

Fig. 3. Struvite contents in the samples precipitated from different solution Ca/Mg molar ratios and pH conditions. The solid symbols represent calculated data based on the Rietveld method, and the dashed lines represent linear fitting lines for different pH conditions. The parameters of these lines are summarized in Table 1.

with the strongest correlation at pH 9.0, as indicated by the correlation coefficients (R^2) in Table 1. The negative slope is a clear indication of the adverse effects of calcium ions on struvite crystallization. A slower drop in struvite contents (with a smaller absolute value of the slope) suggests weaker interference from calcium ion with struvite formation. When all of the curves were fitted with linear correlations, the line for pH 9.0 was found to have the smallest negative slope (absolute value), as shown in Table 1. This finding is consistent with the identification of pH 9.0 as the most favorable environment for struvite crystallization because struvite has the lowest solubility under this condition (Buchanan et al., 1994). When the pH is higher than 9.0, the magnesium phosphate phases may precipitate and interfere with the crystallization of the struvite (Tünay et al., 1997; Ramaru, 2009). In addition to the interference from calcium ions, magnesium phosphate phases may have negative effects on struvite formation under high pH environments. As a result, the curves at pH 10.0 and 11.0 were observed to have larger negative slopes (absolute values) than the lower pH trend lines.

The removal efficiencies of phosphorus, magnesium, and calcium ions from solution to solid phase were also monitored and the results are shown in Fig. 4. The phosphorus removal ratios were higher than 90% for all batch experiments designed in this study (see Fig. 4a). The pH 7.5 sample was observed to have a lower phosphorus removal efficiency than the other pH values, because struvite and calcium phosphates have a higher solubility at pH 7.5. With more calcium introduced into the solution, phosphate species were more effectively removed due to the contribution of calcium phosphate precipitation. Magnesium precipitation declined as the solution's Ca/Mg molar ratio increased. This is similar to the trend of struvite precipitation, indicating that magnesium is primarily precipitated in struvite (see Fig. 4b). However, the highest magnesium precipitation efficiency was at pH 11.0, while the lowest struvite purity was at pH 11.0. This reveals that other magnesium phases were formed in the high pH solutions (pH 10.0 and 11.0). Calcium precipitation efficiency generally remained constant except for a decrease at the Ca/Mg molar ratio of 2:1, because only limited phosphate ions were available for the precipitation reaction (see Fig. 4c). In addition, the precipitated calcium increased as the Ca/Mg ratio increased, as shown in Fig. S1. This explains the high phosphorus removal percentage at a Ca/Mg ratio of 2:1, although both magnesium and calcium ions had low precipitation ratios. Consistent with the precipitation potential analyses in previous studies (Wang et al., 2005; Doyle and Parsons, 2002; Udert et al., 2003), calcium phosphates were more likely to precipitate than struvite when the Ca/Mg ratio was higher than 1:1. A high pH condition may lead to multi-phase precipitates and reduce the purity of struvite, although a high phosphorus removal efficiency may be observed.

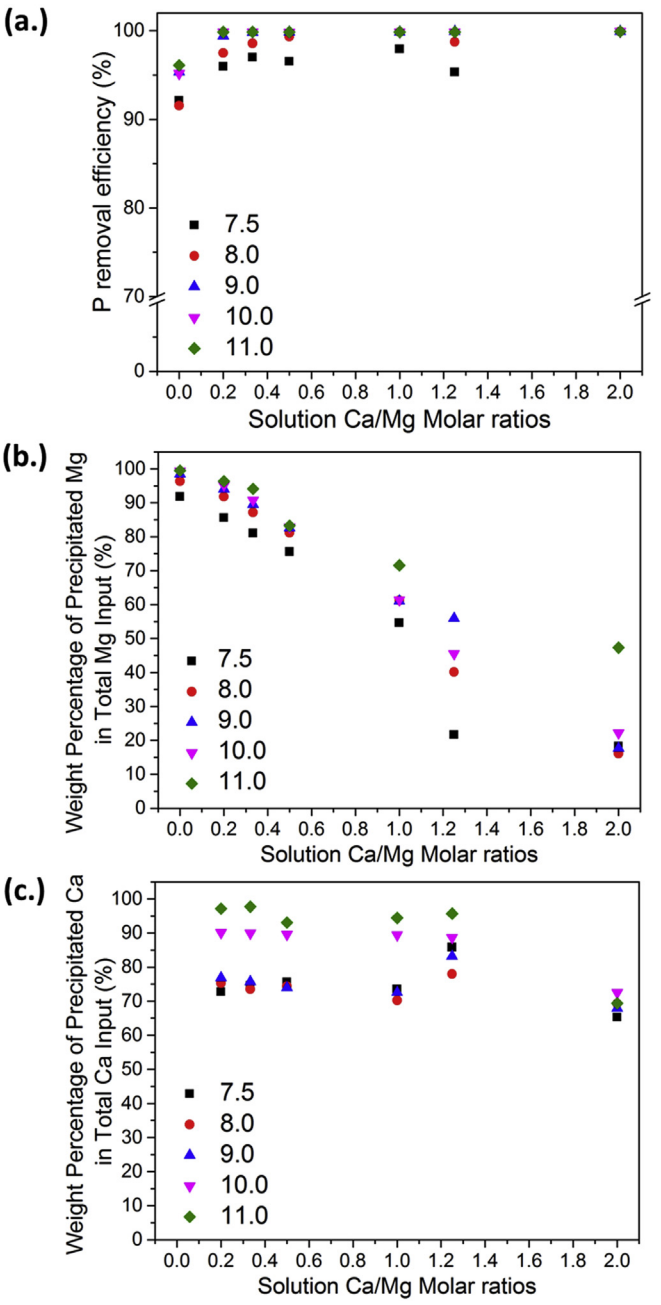

Fig. 4. The change of phosphorus removal efficiency (a), magnesium precipitation efficiency (b) and calcium precipitation efficiency (c) versus solution Ca/Mg molar ratios under different pH conditions.

3.1.2. Analysis of calcium precipitate

As a significant component of the products, calcium precipitate is mostly found in an amorphous form and cannot be completely identified with XRD. Therefore, the analysis of calcium precipitate was clearly delineated with the assistance of SEM, EDS, and Raman

Table 1
Linear regression analysis of struvite weight contents (y, %) versus Ca/Mg molar ratios (x) under different pH values.

pH value	Linear correlation coeff R^2	Slope		Intercept	
		Value	Standard error	Value	Standard error
7.5	0.996	−50.856	1.379	92.540	0.970
8.0	0.981	−50.870	3.169	95.625	2.230
9.0	0.999	−47.064	0.430	91.961	0.302
10.0	0.986	−61.650	3.307	90.084	2.324
11.0	0.998	−71.619	1.462	88.566	1.027

spectroscopy techniques in this study. When observing the morphologic alterations of the struvite particles with SEM (as shown in Fig. 5a–d), we discovered a phenomenon similar to the result of the XRD identification shown in Fig. 1. With a slight addition of calcium, the struvite crystals preferred to grow along the longitudinal axis and finally formed needle-like particles. However, in the presence of comparable calcium ions, the struvite's morphology, including its size and shape, was significantly changed. All of the observed precipitates became irregular, and their surfaces were covered with small particles.

Fig. 5e and f presents the SEM images of the samples precipitated at high Ca/Mg molar ratios at greater magnification. In Fig. 5e, the uneven appearance of struvite particles with obvious cracks reveals the intense influence of calcium on the struvite crystal growth process. Moreover, some accumulated “foreign deposits,” possibly calcium phosphate compounds, were observed on the surface of the obtained struvite precipitates. Most of these foreign deposits were spherical in shape with a diameter of less than 100 nm, as shown in Fig. 5f, which made them easily coagulate from the solution. The EDS mapping analysis further confirmed that the nanoscale deposit was calcium phosphate compound; a typical result is shown in Fig. 6. At pH 8.0, the magnesium precipitate can be considered to be completely struvite; thus, the Mg image denotes the distribution of the struvite particles. Phosphorus was uniformly distributed in the whole precipitates, whereas the calcium image was mainly covered by a pattern of “foreign deposits,” indicating that these irregular precipitates were calcium phosphate phases. Of the common calcium phosphate minerals, hydroxyapatite [HA; $Ca_5(PO_4)_3OH$] is regarded as the most thermodynamically stable form and is precipitated via reaction (5).

$$5Ca^{2+} + 3PO_4^{3-} + OH^- \leftrightarrow Ca_5(PO_4)_3OH(s) \quad (5)$$

However, under homogeneous precipitation, unstable amorphous calcium phosphates should be formed first and then transferred to hydroxyapatite through different approaches depending on the pH environment (House, 1999; Root, 1990). In this study, according to the XRD patterns of the highly amorphous products precipitated from solutions at a Ca/Mg molar ratio of 2:1 (see Fig. 7a), HA was the predominant phase in the precipitates at pH 7.5 and 8.0; in contrast, the HA phase peaks began to disappear from the XRD pattern as the pH exceeded 9.0. Two potential explanations are proposed here: the transition of the amorphous calcium phosphates to the HA was blocked at high pH conditions, or compounds other than calcium phosphates were formed as the major composition of the precipitates when the pH increased. The broadening of the peak in the samples at pH 7.5 and 8.0 was probably due to the small particle size of the HA crystals, which are generally in the nanometer scale. To further understand the alteration in the highly amorphous samples, Raman spectroscopy was performed to analyze the elemental and structural information of two selected samples obtained at pH 7.5 and 11.0 (see Fig. 7b). The Raman spectra of both samples corresponded well to the HA spectrum (Silva and Sombra, 2004). Applying the same test parameters, Raman spectroscopy was used to provide a rough evaluation of the amount of hydroxyapatite in the total product. When the pH was increased to 11.0, the intensities of the typical hydroxyapatite peaks located at 428 cm^{-1}, 579 cm^{-1}, 591 cm^{-1}, and 960 cm^{-1} were obviously reduced. Thus, consistent with the XRD result in Fig. 7a, the Raman spectra showed a significant decrease in the hydroxyapatite content in the products precipitated from high-pH environments. Combined with the elemental analysis of the corresponding samples by EDS, as shown in Fig. 7c, the amount of magnesium in the product achieved at pH 11.0 was greater than that obtained at pH 7.5, although oxygen, calcium, and phosphorus were the major elements in both samples. This finding suggests that calcium phosphates were still the major components of the products precipitated from the high-pH solutions, but in the form of amorphous calcium phosphate rather than hydroxyapatite. High pH (pH $\geq$ 10.0) decreases the supersaturation level of hydroxyapatite in solution, extending the induction time of amorphous calcium phosphate to HA conversion (Boskey and Posner, 1973). Moreover, magnesium was increasingly precipitated in phosphate and other forms at higher pH values. To further identify the magnesium phases, the equilibrium distribution of the phosphorus species versus the solution pH was analyzed according to the dissolution and hydrolysis reaction of KH_2PO_4 in aqueous solution, which can be expressed by Eqs (6)–(8):

$$KH_2PO_4 \rightarrow K^+ + H_2PO_4^- \quad (6)$$

$$H_2PO_4^- \leftrightarrow H^+ + HPO_4^{2-} \quad \left(K_2 = 6.31 \times 10^{-8}\right) \quad (7)$$

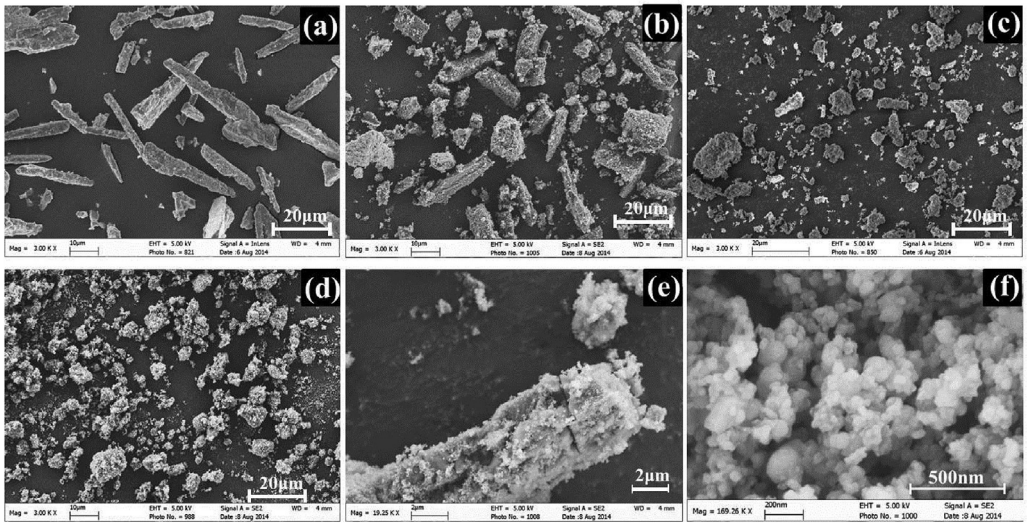

Fig. 5. SEM images of precipitates obtained in experiments at pH 10.0. The Ca/Mg ratios are of 1:5 (a), 1:2 (b and e), 1:1 (c) and 2:1 (d and f).

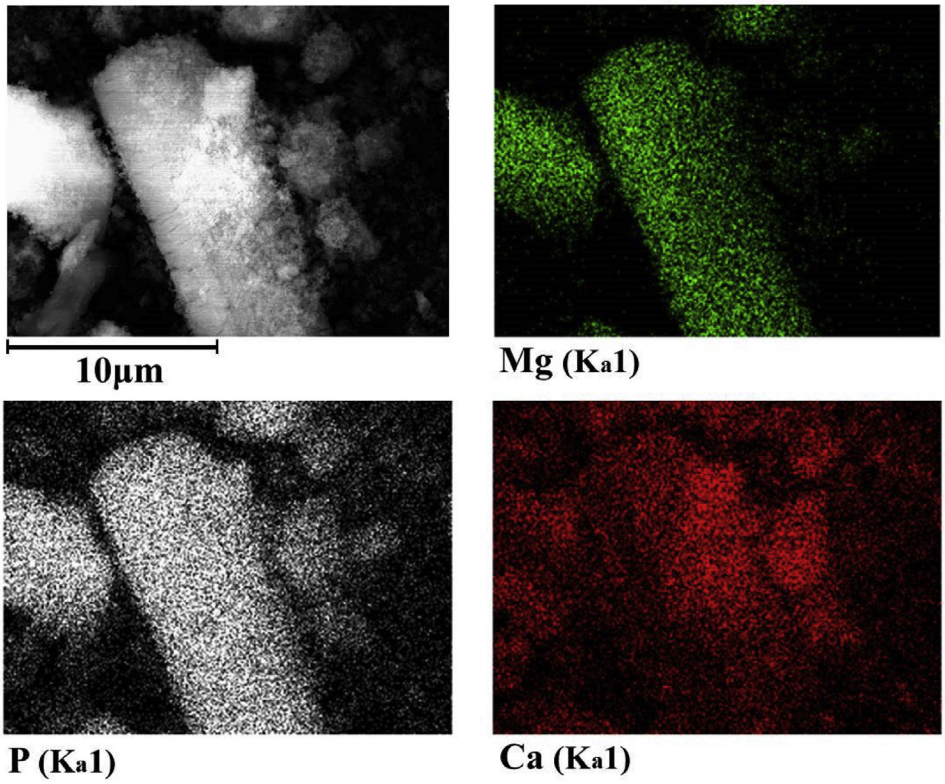

Fig. 6. EDS mapping result of Mg, P and Ca in the sample precipitated from the solution with Ca/Mg ratio of 1:1 under pH 8.0. The corresponding SEM image is shown in the left top corner.

$$HPO_4^{2-} \leftrightarrow H^+ + PO_4^{3-} \quad \left(K_3 = 4.8 \times 10^{-13}\right) \tag{8}$$

where K_2 and K_3 refer to the phosphoric acid dissociation constants K_{a2} and K_{a3}, respectively. Fig. S2 shows that HPO_4^{2-} was predominant in all of the studied pH environments and that the concentration of PO_4^{3-} ions increased significantly when the pH exceeded 9.0, resulting in supersaturation of the magnesium phosphate phases. Consistent with the studies of Tünay et al. (1997) and Ramaru (2009), the magnesium phosphate phases (probably including $Mg_3PO_4 \cdot 22H_2O$ and $Mg_3PO_4 \cdot 6H_2O$) were precipitated from the studied solution under high-pH conditions and interfered with the crystallization of struvite and hydroxyapatite. The results demonstrate that pH plays an important role in determining the effect of calcium ions on struvite crystallization because the precipitation of magnesium and calcium phosphate is sensitive to pH. On the basis of this discussion, it can be concluded that a high-pH environment (pH $\geq$ 10.0) has negative effects on both struvite and hydroxyapatite precipitation.

3.2. Influence of iron ions on struvite crystallization

The concentration of Fe^{3+} in the ferric ion condition cannot be comparable to that of Mg^{2+} in wastewater due to its extremely limited solubility. In general, additives with dosages of less than 10 ppm are not considered to significantly interfere with the main chemical characteristics and functions of solutions (Muryanto and Bayuseno, 2014; Hasson and Semiat, 2006). Therefore, ferric concentrations of 1 ppm and 5 ppm were selected to investigate the role of ferric ions during the struvite crystallization process. Ferric concentrations of 100 ppm and 200 ppm were also studied to assess the effects of elevated iron concentrations in the systems. In addition, to compare the influences of the ferric ions and calcium ions on struvite crystallization, the dosage of ferric chloride was designated with an Fe:Mg molar ratio of 1:5 (concentration of Fe^{3+} at 372 ppm). The products precipitated from the solutions with $FeCl_3$ were light yellow, indicating that the ferric precipitates were incorporated into the struvite products. The quantitative XRD analysis and Topas results are presented in Fig. 8. With limited addition (1 ppm and 5 ppm), ferric ions (Fe^{3+}) did not show a clear influence on the amount of struvite generated. However, as the ferric dosage increased, the prohibitive effects became pronounced. Within the experimental pH range, aqueous Fe(III) ions existed in three dominant species, $Fe(OH)_2^+$, $Fe(OH)_3(aq)$, and $Fe(OH)_4^-$, all at concentrations of less than 10^{-10} M (equivalent to 5.6×10^{-3} ppm-Fe) (Stumm and Morgan, 2012), indicating that more than 99% of the dosed iron was precipitated. It is thus unlikely that the aqueous ferric species directly participated in and affected the struvite crystallization. However, the ferric precipitation might have considerably reduced the phosphate concentrations in the solutions, largely initiated by the precipitation of ferric phosphates, leading to the decrease in struvite production particularly with high ferric doses ($\geq$100 ppm). When the Fe:Mg molar ratio reached 1:5, the struvite weight percentages among the whole precipitates were 60% and 69% for pH 7.5 and pH 9.0, respectively, whereas the corresponding struvite contents (with Ca/Mg at 1:5) in the calcium experiments were 83% and 82%. Obviously, under the same conditions, ferric ions prohibit struvite crystallization more seriously than do calcium ions, suggesting that ferric ions could be more efficient inhibitors of struvite formation. This utility is attributable to the stronger binding ability of ferric ion (Fe^{3+}) than calcium ion (Ca^{2+}) with phosphorus species. Due to the hydrolysis reaction of Fe^{3+} and the acid/base equilibrium of phosphoric acid, the ferric

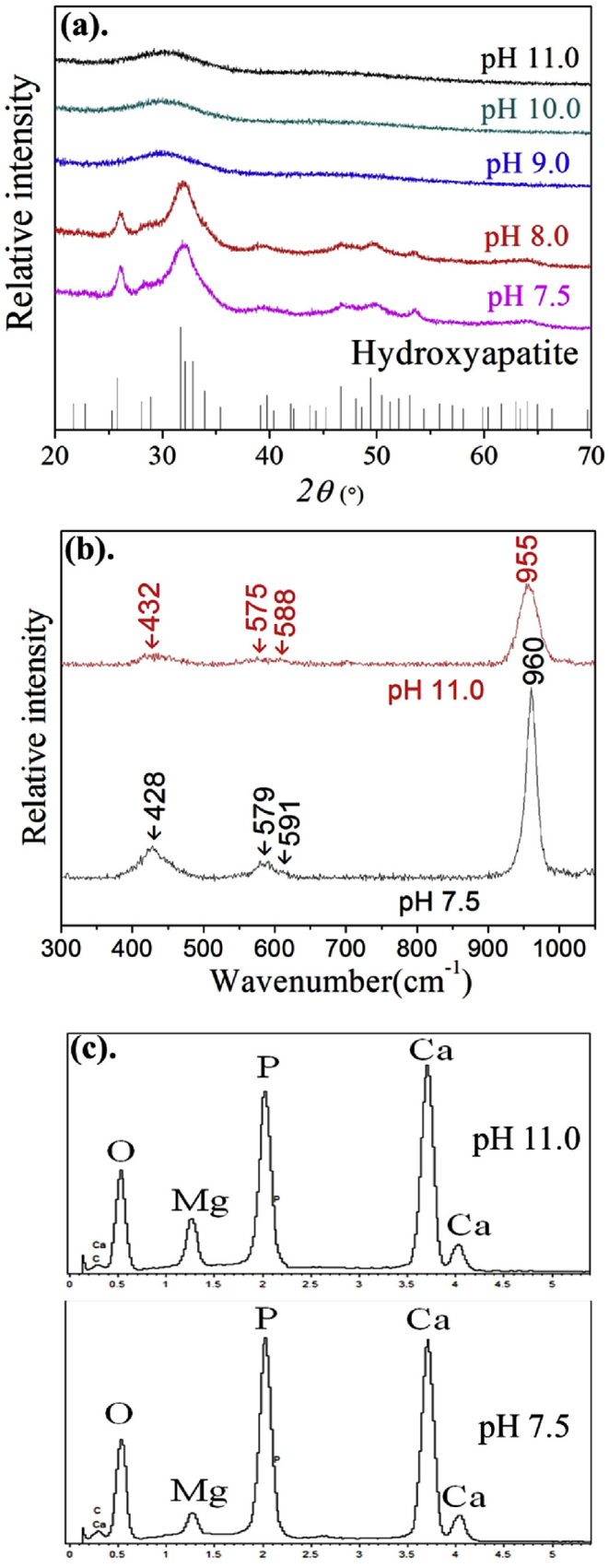

Fig. 7. (a) XRD patterns of precipitates with the initial Ca/Mg molar ratio of 2:1 at various pH conditions and the standard hydroxyapatite pattern (HA, PDF#09-0432); (b) Raman spectra of the samples obtained from solution with a Ca/Mg ratio of 2:1 at pH 7.5 and 11.0; (c) EDS spectra of the corresponding samples in (b).

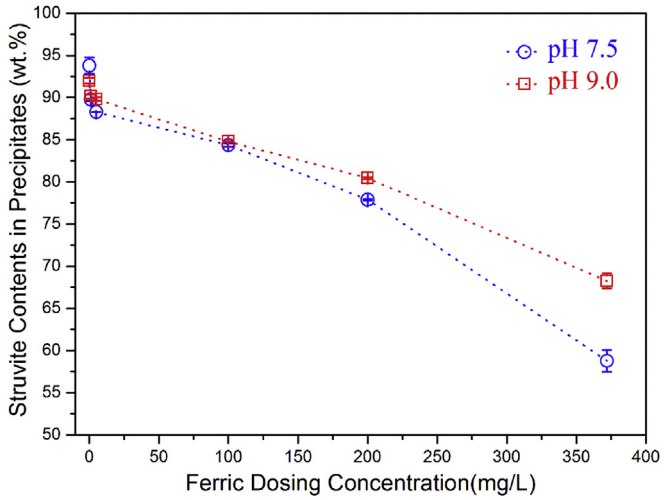

Fig. 8. Struvite contents in the samples precipitated from solutions with different ferric dosages and pH conditions.

phosphate precipitation process is especially complex and difficult to define. Luedecke et al. (1989) proposed a chemical model to describe the ferric hydroxyl-phosphate precipitation either alone or in combination with ferric hydroxide formation in activated sludge. They found that the ferric hydroxyl-phosphate deposit could be expressed by an empirical formula, $Fe_{2.5}PO_4(OH)_{4.5}$, with a calculated solubility product constant at pKsp = 96.7, whereas the corresponding solubility constants for struvite (MAP) and hydroxyapatite (HA) are pK_{MAP} = 13.26 (Ohlinger et al., 1998) and pK_{HA} = 58.69 (Markovic et al., 2004), respectively. In addition, the co-precipitates of ferric phosphate and ferric hydroxide adsorbed some phosphate ions to further remove phosphorus species from the solution. These factors greatly enhanced the P-removal ability of $FeCl_3$, which was much more effective than $CaCl_2$, and consistently more pronounced effects on struvite crystallization were observed. Similar to the results of the calcium addition experiments, struvite was less affected by the addition of ferric ions at pH 9.0 than at pH 7.5 in the overall trend. The pH value of 9.0 was again confirmed as the most suitable for struvite crystallization.

Despite the slight effect on the quantity of struvite with the addition of 100 ppm and 200 ppm ferric contents, ferric ions were found to influence the morphology of struvite by hindering the growth of some crystal planes (see Fig. 9). The addition of $FeCl_3$ changed the needle-like precipitates into an irregular shape, mainly as a result of suppressed growth in the longitudinal direction. In addition, the smooth surfaces of the precipitates became rough with cracks, probably due to the incorporated and/or adsorbed foreign ions. Because the ferric precipitates were formed earlier than struvite at a lower pH, they may have acted as nuclei that led to the struvite crystal clusters observed in the SEM images, as shown in Fig. 9.

Another interesting and widely discussed question concerns whether foreign ions can be incorporated into the struvite structure. Lin et al. (2013) confirmed the incorporation of arsenic ions in struvite by means of synchrotron X-ray absorption spectroscopy and electron paramagnetic resonance spectroscopy. In contrast, Ma and Rouff (2012) reported that the co-precipitation of As(V) and the adsorption of As(III) were the major mechanisms for the incorporation of arsenic into mineralized struvite. Similarly, Muryanto and Bayuseno (2014) reported that Cu^{2+} and Zn^{2+} affected struvite crystallization by physical adsorption. Although the mechanisms of the effect of Fe^{3+} on the crystallization of struvite are not yet fully

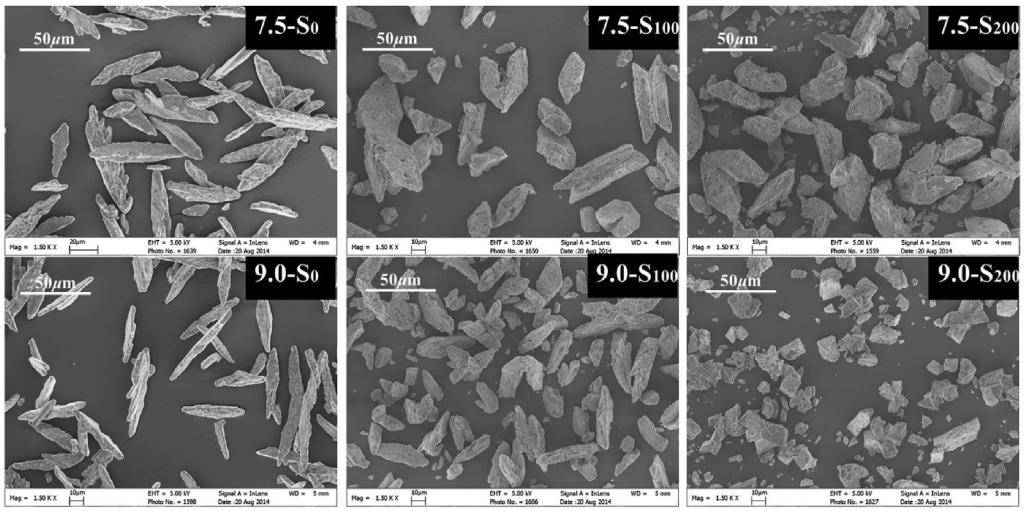

Fig. 9. Secondary electron images of the precipitates obtained from experiments with different ferric dosages at pH 7.5 and pH 9.0. S_0, S_{100}, and S_{200} are samples with the addition of 0 ppm, 100 ppm, and 200 ppm Fe^{3+}, respectively.

elucidated, the similar lattice parameters and cell volumes derived from the XRD data in this study, as presented in Table S3, suggest that the accumulation (adsorption) of ferric ions on the struvite crystal surfaces may be responsible, rather than lattice incorporation.

4. Conclusion

As struvite is precipitated and crystallized from aqueous solutions, it is important to evaluate the effect of foreign ions, especially those that commonly exist in wastewater, on the struvite crystallization process. This study applied a quantitative XRD technique to access the influences of calcium (Ca^{2+}) and ferric (Fe^{3+}) ions on struvite formation in solutions of different compositions and pH values. The quantification results demonstrated that the struvite crystallization was significantly inhibited by the co-existence of calcium ions, and the prohibitory effect had a negative linear correlation. The hydroxyapatite phase was predominant in the highly amorphous samples precipitated from pH 7.5 and 8.0, while its quantity decreased at higher pH values, presumably due to the precipitation of other calcium phosphate and magnesium phosphate phases. At limited dosages, ferric ions (Fe^{3+}) had a clear influence on struvite formation, confirming it to be a more effective inhibitor of struvite production than calcium ions. Surface adsorption is suggested as the main mechanism by which Fe^{3+} affects the crystallization of struvite, based on the very similar lattice parameters obtained from the XRD data analysis. The overall outcomes of this study indicate that the effective control of foreign ions (Ca^{2+} and Fe^{3+}) in solutions is essential to recover high-quality struvite products from waste streams.

Acknowledgements

We gratefully acknowledge the funding for this research provided by the General Research Fund Scheme of the Research Grants Council of Hong Kong (715612, 17206714), HKU Strategic Research Themes on Clear Energy and Earth as a Habitable Planet.

Appendix A. Supplementary data

Supplementary data related to this article can be found at http://dx.doi.org/10.1016/j.watres.2016.03.032.

References

Battistoni, P., De Angelis, A., Prisciandaro, M., Boccadoro, R., Bolzonella, D., 2002. P removal from anaerobic supernatants by struvite crystallization: long term validation and process modelling. Water Res. 36 (8), 1927–1938.
Borgerding, J., 1972. Phosphate deposits in digestion systems. J. Wat. Pollut. Control Fed. 44 (5), 813–819.
Boskey, A.L., Posner, A.S., 1973. Conversion of amorphous calcium phosphate to microcrystalline hydroxyapatite. A pH-dependent, solution-mediated, solid-solid conversion. J. Phys. Chem. 77 (19), 2313–2317.
Buchanan, J., Mote, C., Robinson, R., 1994. Thermodynamics of struvite formation. In: Transactions of the ASAE (USA).
Charles, W., Cord-Ruwisch, R., Ho, G., Costa, M., Spencer, P., 2006. Solutions to a combined problem of excessive hydrogen sulfide in biogas and struvite scaling. Water Sci. Technol. 53 (6), 203–210.
Cusick, R.D., Ullery, M.L., Dempsey, B.A., Logan, B.E., 2014. Electrochemical struvite precipitation from digestate with a fluidized bed cathode microbial electrolysis cell. Water Res. 54, 297–306.
Doyle, J.D., Parsons, S.A., 2002. Struvite formation, control and recovery. Water Res. 36 (16), 3925–3940.
Ge, H., Zhang, L., Batstone, D.J., Keller, J., Yuan, Z., 2012. Impact of iron salt dosage to sewers on downstream anaerobic sludge digesters: sulfide control and methane production. J. Environ. Eng. 139 (4), 594–601.
Guirado, F., Galı, S., Chinchón, S., 2000. Quantitative Rietveld analysis of aluminous cement clinker phases. Cem. Concr. Res. 30 (7), 1023–1029.
Gutierrez, O., Park, D., Sharma, K.R., Yuan, Z., 2010. Iron salts dosage for sulfide control in sewers induces chemical phosphorus removal during wastewater treatment. Water Res. 44 (11), 3467–3475.
Hasson, D., Semiat, R., 2006. Scale control in saline and wastewater desalination. Israel J. Chem. 46 (1), 97–104.
House, W.A., 1999. The physico-chemical conditions for the precipitation of phosphate with calcium. Environ. Technol. 20 (7), 727–733.
Kabdaszli, I., Parsons, S.A., Tünaya, O., 2006. Effect of major ions on induction time of struvite precipitation. Croat. Chem. Acta 79 (2), 243–251.
Le Corre, K., Valsami-Jones, E., Hobbs, P., Parsons, S., 2009. Phosphorus recovery from wastewater by struvite crystallization: a review. Crit. Rev. Environ. Sci. Technol. 39 (6), 433–477.
Le Corre, K.S., Valsami-Jones, E., Hobbs, P., Parsons, S.A., 2005. Impact of calcium on struvite crystal size, shape and purity. J. Cryst. Growth 283 (3), 514–522.
Lin, J., Chen, N., Pan, Y., 2013. Arsenic incorporation in synthetic struvite ($NH_4MgPO_4 \cdot 6H_2O$): a synchrotron XAS and single-crystal EPR study. Environ. Sci. Technol. 47 (22), 12728–12735.
Luedecke, C., Hermanowicz, S.W., Jenkins, D., 1989. Precipitation of ferric phosphate in activated sludge: a chemical model and its verification. Water Sci. Technol. 21 (4–5), 325–337.
Ma, N., Rouff, A.A., 2012. Influence of pH and oxidation state on the interaction of arsenic with struvite during mineral formation. Environ. Sci. Technol. 46 (16), 8791–8798.
Mamais, D., Pitt, P.A., Cheng, Y.W., Loiacono, J., Jenkins, D., 1994. Determination of ferric chloride dose to control struvite precipitation in anaerobic sludge digesters. Water Environ. Res. 912–918.
Markovic, M., Fowler, B.O., Tung, M.S., 2004. Preparation and comprehensive characterization of a calcium hydroxyapatite reference material. J. Res. Natl. Inst. Stand. Technol. 109 (6), 553–568.
Massey, M.S., Davis, J.G., Sheffield, R.E., Ippolito, J.A., 2007. Struvite production from

dairy wastewater and its potential as a fertilizer for organic production in calcareous soils. In: American Society of Agricultural and Biological Engineers, p. 23.
Moerman, W., Carballa, M., Vandekerckhove, A., Derycke, D., Verstraete, W., 2009. Phosphate removal in agro-industry: pilot-and full-scale operational considerations of struvite crystallization. Water Res. 43 (7), 1887–1892.
Mullin, J.W., 1972. Crystallisation. Butterworths, London.
Muryanto, S., Bayuseno, A., 2014. Influence of Cu2+ and Zn2+ as additives on crystallization kinetics and morphology of struvite. Powder Technol. 253, 602–607.
Musvoto, E., Wentzel, M., Ekama, G., 2000. Integrated chemical–physical processes modelling—II. Simulating aeration treatment of anaerobic digester supernatants. Water Res. 34 (6), 1868–1880.
Ohlinger, K., Young, T., Schroeder, E., 1998. Predicting struvite formation in digestion. Water Res. 32 (12), 3607–3614.
Parsons, S., Wall, F., Doyle, J., Oldring, K., Churchley, J., 2001. Assesing the potential for struvite recovery at sewage treatment works. Environ. Technol. 22 (11), 1279–1286.
Pitman, A., Deacon, S., Alexander, W., 1991. The thickening and treatment of sewage sludges to minimize phosphorus release. Water Res. 25 (10), 1285–1294.
Rahman, M.M., Salleh, M.A.M., Rashid, U., Ahsan, A., Hossain, M.M., Ra, C.S., 2014. Production of slow release crystal fertilizer from wastewaters through struvite crystallization – a review. Arabian J. Chem. 7 (1), 139–155.
Ramaru, R., 2009. Phosphate Precipitation as Struvite from Municipality Wastewater. University of Cape Town.
Rawn, A., Banta, P., Pomeroy, R., 1939. Multiple stage sewage digestion. Trans. Am. Soc. Agric. Eng. 105, 93–132.
Root, M.J., 1990. Inhibition of the amorphous calcium phosphate phase transformation reaction by polyphosphates and metal ions. Calcif. Tissue Int. 47 (2), 112–116.
Rouff, A.A., 2013. Temperature-dependent phosphorus precipitation and chromium removal from struvite-saturated solutions. J. Colloid Interface Sci. 392, 343–348.
Silva, C., Sombra, A., 2004. Raman spectroscopy measurements of hydroxyapatite obtained by mechanical alloying. J. Phys. Chem. Solids 65 (5), 1031–1033.
Stumm, W., Morgan, J.J., 2012. Aquatic Chemistry: Chemical Equilibria and Rates in Natural Waters. John Wiley & Sons.
Sutor, D., Wooley, S.E., 1972. The structure and formation of urinary calculi: I. Oriented crystal growth. Br. J. Urol. 44 (5), 532–536.
Tünay, O., Kabdasli, I., Orhon, D., Kolçak, S., 1997. Ammonia removal by magnesium ammonium phosphate precipitation in industrial wastewaters. Water Sci. Technol. 36 (2), 225–228.
Udert, K.M., Larsen, T.A., Gujer, W., 2003. Estimating the precipitation potential in urine-collecting systems. Water Res. 37 (11), 2667–2677.
Wang, J., Burken, J.G., Zhang, X.J., 2006. Effect of seeding materials and mixing strength on struvite precipitation. Water Environ. Res. 78 (2), 125–132.
Wang, J., Burken, J.G., Zhang, X.J., Surampalli, R., 2005. Engineered struvite precipitation: impacts of component-ion molar ratios and pH. J. Environ. Eng. 131 (10), 1433–1440.
Wiles, D.T., Young, R., 1981. A new computer program for Rietveld analysis of X-ray powder diffraction patterns. J. Appl. Crystallogr. 14 (2), 149–151.
Williams, S., 1999. Struvite precipitation in the sludge stream at Slough wastewater treatment plant and opportunities for phosphorus recovery. Environ. Technol. 20 (7), 743–747.
Young, R., 1993. The Rietveld Method, IUCr. Monographs on Crystallography. Oxford University Press, Oxford.